Grid-independent large-eddy simulation using explicit filtering

Sanjeeb T. Bose, Parviz Moin, and Donghyun You

Citation: Physics of Fluids **22**, 105103 (2010);
View online: https://doi.org/10.1063/1.3485774
View Table of Contents: http://aip.scitation.org/toc/phf/22/10
Published by the American Institute of Physics

Grid-independent large-eddy simulation using explicit filtering

Sanjeeb T. Bose,[1] Parviz Moin,[1] and Donghyun You[2]
[1]*Center for Turbulence Research, Stanford University, California 94305-4035, USA*
[2]*Department of Mechanical Engineering, Carnegie Mellon University, Pennsylvania 15213-3890, USA*

(Received 16 November 2009; accepted 25 May 2010; published online 21 October 2010)

The governing equations for large-eddy simulation are derived from the application of a low-pass filter to the Navier–Stokes equations. It is often assumed that discrete operations performed on a particular grid act as an implicit filter, causing results to be sensitive to the mesh resolution. Alternatively, explicit filtering separates the filtering operation, and hence the resolved turbulence, from the underlying mesh distribution alleviating some of the grid sensitivities. We investigate the use of explicit filtering in large-eddy simulation in order to obtain numerical solutions that are grid independent. The convergence of simulations using a fixed filter width with varying mesh resolutions to a true large-eddy simulation solution is analyzed for a turbulent channel flow at $\mathrm{Re}_\tau=180$, 395, and 640. By using explicit filtering, turbulent statistics and energy spectra are shown to be independent of the mesh resolution used. © *2010 American Institute of Physics*.
[doi:10.1063/1.3485774]

I. INTRODUCTION

Large-eddy simulation (LES) directly solves for large-scale motions in turbulent flow while modeling the influence of small-scale eddies. Recent studies have shown that LES provides a tractable method for the simulation of turbulent flows at high Reynolds numbers in complex geometries.[1–3] The governing LES equations are derived by the application of a low-pass filter, G, to the Navier–Stokes equations,

$$\bar{u}_i(x_i,t)=\int_\Omega G(x_i,x_i',\Delta)u_i(x_i',t)dx_i', \tag{1}$$

$$\frac{\partial \bar{u}_i}{\partial t}+\frac{\partial \bar{u}_i\bar{u}_j}{\partial x_j}=-\frac{\partial \bar{p}}{\partial x_i}+\frac{1}{\mathrm{Re}}\frac{\partial^2\bar{u}_i}{\partial x_j\,\partial x_j}-\frac{\partial \tau_{ij}}{\partial x_j}, \tag{2}$$

$$\frac{\partial \bar{u}_i}{\partial x_i}=0, \tag{3}$$

where u_i is the vector of velocities, p is the pressure, Δ denotes some measure of the filter width, $\tau_{ij}=\overline{u_iu_j}-\bar{u}_i\bar{u}_j$, and commutation of the differentiation and filtering operators is assumed. Although the filtering operation is unambiguously defined in deriving Eq. (2), in most numerical simulations the filter is not defined. It is assumed that the attenuation of high wavenumbers present in most finite difference/finite volume schemes acts as a low-pass filter,[4]

$$\frac{1}{2\Delta x}\int_{x_{i-1}}^{x_{i+1}}\frac{du}{dx'}dx'=\frac{u_{i+1}-u_{i-1}}{2\Delta x}=\overline{\left.\frac{du}{dx}\right|_{x_i}}. \tag{4}$$

Thus, if provided with a closure model for the subgrid stress tensor $\tau_{ij}=f(\bar{u}_i,\bar{u}_j)$ and an initial condition for $\bar{u}_i$, it is possible to advance the solution for the filtered variables in time without defining the filtering operation. However, it has been shown[5] that the equivalence of discretized operators and filtering is inconsistent with the derivation of filtered Navier–Stokes equations. One of the difficulties associated with the arguments for implicitly filtered (or traditional) LES is that the filtering is performed only in the direction in which the derivative (or interpolation) is applied. Hence, each term in the LES equation is subjected to a different one-dimensional (1D) filter, and the actual equation being solved cannot be rigorously derived from the Navier–Stokes equations. Owing to the inherent dependence of the filtering operation on the discretized operators, it is not surprising that solutions of implicitly filtered LES are extremely sensitive to the numerical grid used. Kravchenko and Moin[6] found that for turbulent flow around a cylinder at $\mathrm{Re}_D=3900$, a coarser spanwise resolution could produce better agreement with experimental data. Similarly, Meyers and Sagaut[7] observed that the streamwise and spanwise resolutions could be coarsened such that the wall shear stress was correctly calculated in a turbulent channel flow. For some LES solutions, grid refinement causes the agreement with direct numerical simulation or experimental data to deteriorate.

In practice, a sequence of solutions is obtained on successively finer meshes until a sufficient range of scales in the flow field has been resolved and the statistical quantities of interest are invariant with respect to the mesh. This process is often referred to as grid convergence. However, the grid-converged solution of the implicitly filtered LES is not the true solution of the LES equations. Rather, the true LES solution corresponds to the filtered velocity field, given a particular closure model and a well-defined spatial filter. In the limit when the mesh size is sufficiently small to capture the smallest scales of motion, an implicitly filtered LES will converge to a direct numerical simulation because the filter width also approaches the size of the smallest eddy. This limit, of course, is unreachable in most practical situations where LES is applied.

LES is also particularly sensitive to numerical error. In most numerical simulations of physical phenomena, the detrimental impact of numerical errors can be avoided by choosing a mesh size much smaller than the smallest dy-

namically relevant length scale. This is difficult for many turbulent flows regardless of the numerical method used. Kravchenko and Moin[8] demonstrated that the performance of the subgrid stress model could be impeded due to the truncation error as the energy spectrum at higher wavenumbers becomes distorted. *A priori* analyses of direct numerical simulation data of stably stratified shear flow demonstrated that both the truncation and aliasing errors associated with a numerical scheme could independently dominate the contribution of the subgrid stress tensor.[9]

Explicit filtering re-emerged a decade ago as a method to rigorously derive the constitutive equations for the large-scale field and to separate the filtering and discretization operators.[5,10,11] However, several difficulties impeded its widespread implementation. In virtually all derivations of the LES equations, the filtering operation is assumed to commute with differentiation, and thus, any explicit filter used in a numerical simulation must also commute with differentiation. Vasilyev *et al.*[12] derived filters that can commute with differentiation on nonuniform meshes to the order of accuracy of the numerical scheme. Further development of this general class of commuting filters by Marsden *et al.*[13] and Haselbacher and Vasilyev[14] extended their applicability to unstructured meshes. Another criticism of explicit filtering has been the sensitivity of the LES solution to the particular filter employed. Large-eddy simulation, both implicitly filtered and explicitly filtered, is predicated upon the choice of a spatially varying length scale that would capture the large, energy-containing eddies throughout a turbulent flow. Traditionally, this length scale is imposed by refining the grid near solid boundaries where the dynamically important eddies are expected to be smaller. Explicitly filtered LES prescribes a filter whose width decreases near solid boundaries in order to capture the energy-containing eddies. The effect of the choice of filter (or local length scale) is not unique to explicitly filtered LES;[15] however, it is expected that if most of the energy is captured, the turbulent statistics should be relatively insensitive to the particular choice of filter. Second, the two approaches to specifying the local length scale are not equivalent. In the former case where the length scale is prescribed indirectly through the grid size, it is impossible to isolate the numerical error present in the LES solution.

To date only a handful of explicitly filtered LES simulations have been performed. The initial use of explicit filtering in LES was in conjunction with solving an inverse problem for the unfiltered variables, u_i, from the filtered quantities, $\bar{u}_i$. Winckelmans *et al.*[16] implemented a two-dimensional (2D) explicit filter for isotropic turbulence and channel flow in evaluating the performance of various mixed models. Stolz *et al.*[17] implemented the filtering schemes of Vasilyev *et al.*[12] in using an approximate deconvolution model for the convective terms in the LES equations, including the construction of filtering operators in all three dimensions. Lund[5] implemented 2D explicit filters for a channel flow and evaluated the performance of explicitly filtered versus implicitly filtered LES for a variety of models. However, Lund mixed explicit filtering along homogeneous directions and implicit filtering along the wall-normal direction. Commutation between the filtering and differentiation operators along inhomogeneous directions when the filter width varies is not trivially satisfied, and one-sided filters need to be employed near solid boundaries. Gullbrand[10] attempted the first grid-independent solution of the LES equations with explicit filtering. However, the explicit filter used on the finer meshes was inconsistent with the filter used on the coarser meshes, and the statistics obtained were not conclusively grid independent.

The objective of the present study is to obtain grid-independent solutions of the governing equations for large-eddy simulation. A truly grid-independent solution is one such that the numerical errors, both the truncation and commutation errors, are sufficiently small that the turbulent statistics demonstrate that a grid-converged solution has been reached. Note that the performance of explicitly filtered LES with respect to direct numerical simulation or experimental data is not within the scope of this discussion. If the flow statistics of the grid-independent solution of the explicitly filtered LES equations are not in good agreement with filtered direct numerical simulation (DNS) statistics, this failure can be attributed solely to the capability of the subfilter stress model employed. Section II constructs the mathematical framework for explicitly filtered LES, Sec. III presents results from explicitly filtered LES of a turbulent channel flow at different Reynolds numbers, and Sec. IV contains a few concluding remarks.

II. MATHEMATICAL FRAMEWORK

A. Explicitly filtered LES

The convective term in the governing equations for LES can be recast in an equivalent form,

$$\frac{\partial \bar{u}_i}{\partial t} + \frac{\partial \overline{\bar{u}_i \bar{u}_j}}{\partial x_j} = -\frac{\partial \bar{p}}{\partial x_i} + \frac{1}{\mathrm{Re}} \frac{\partial^2 \bar{u}_i}{\partial x_j \partial x_j} - \frac{\partial \tau_{ij}}{\partial x_j}, \tag{5}$$

$$\tau_{ij} = \overline{u_i u_j} - \overline{\bar{u}_i \bar{u}_j}, \tag{6}$$

with the remaining condition that the filtered velocity field, $\bar{u}_i$, is solenoidal. This form of the LES equations explicitly accounts for the Leonard term (see Ref. 18) and consistently confines the bandwidth of all the terms in the governing equation to those dictated by the filter, if the filter has a well-defined cutoff. For filters without a well-defined cutoff, the filtering operator will still project the terms in the governing equation onto the space spanned by the filter kernel, $G(x,x')$. The resolved motions are thus the range of the filter kernel, whereas the unresolved motions correspond to the null space of the kernel. This form of the equation also includes the explicit presence of the filter in the LES equations. Moreover, the filtering operator is no longer implicitly defined by the particular grid used, and filtering and discretization operations are formally separated. The unclosed term in Eq. (6) is referred to as the subfilter stress because it is responsible for the effect of scales smaller than the filter width on the resolved scales. In contrast, the unclosed term τ_{ij} in Eq. (2) is referred to as a subgrid stress because it accounts for the effects of scales smaller than the grid size on the resolved scales. The remaining constraint on the filtering op-

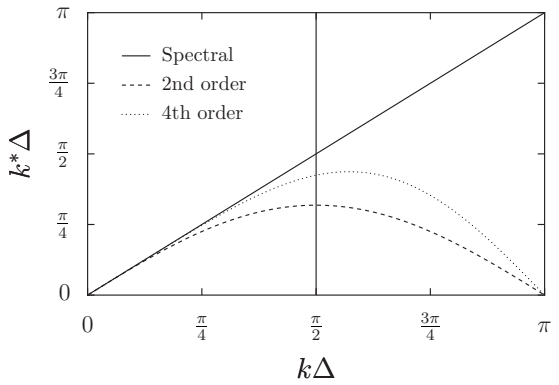

FIG. 1. Modified wavenumbers for second- and fourth-order central differences shown with a hypothetical cutoff filter at $k\Delta=\pi/2$.

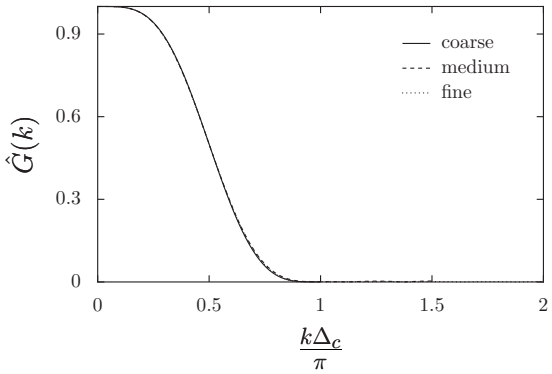

FIG. 2. Fourier transform of filter functions $\hat{G}(k)$ with respect to a nondimensional wavenumber for a coarse grid, $\Delta_c k$. Medium grid, $\Delta_m=\frac{2}{3}\Delta_c$, and fine grid, $\Delta_f=\frac{1}{2}\Delta_c$, transfer functions are constructed to match that of the coarse grid.

erator is that it must commute with differentiation,

$$\left[\frac{\partial f}{\partial x}\right] = \overline{\frac{\partial f(x)}{\partial x}} - \frac{\partial \overline{f(x)}}{\partial x} = \epsilon, \tag{7}$$

where ϵ is sufficiently small. Vasilyev *et al.*[12] proposed a filter kernel of the form

$$\frac{1}{\Delta}G(x',x) = \sum_{j=-K}^{L} w_j \delta(x'-j\Delta), \tag{8}$$

which is a linear combination of Dirac delta functions, $\delta(x')$, with weight w_j over the interval $x' \in [x-L\Delta, x+K\Delta]$. The filtering operator applied to some function, ϕ, with the kernel in Eq. (8) can be equivalently expressed as a discrete filter,

$$\bar{\phi}(x) = \int G(x',x)\phi(x')dx' = \sum_{j=-K}^{L} w_j \phi(x-j\Delta). \tag{9}$$

This filtering operator does not satisfy Eq. (7) exactly, but by proper choice of the weights, w_j can satisfy Eq. (7) to an arbitrary order of accuracy, $[\partial f/\partial x]=O(\tilde{\Delta}^p)$. The order of commutation, p, is chosen to be the same order as the truncation error of the numerical scheme used and $\tilde{\Delta}$ corresponds to the uniform grid spacing in the mapped space. Because Eq. (7) is not satisfied exactly, it is assumed that the closure model provided for $\partial\tau_{ij}/\partial x_j$ also models the effect of the remaining commutation error terms. Note that these terms are only dependent on the choice of the filter and not on the computational grid.

In the above derivation, the choice of the filter is arbitrary provided that it commutes with differentiation. Standard finite difference and finite volume operators have large numerical errors that are concentrated at high wavenumbers, and thus, the filter kernel can be chosen in order to damp high wavenumbers that would be contaminated by the truncation error.[19] Figure 1 shows the modified wavenumbers for second- and fourth-order central difference operators and a hypothetical cutoff filter; the filter cutoff depicted can preserve the range of wavenumbers that are adequately resolved by the discrete difference operator and damp the higher

TABLE I. Numerical parameters for channel flow simulations. N_x, N_y, and N_z denote the number of grid points used in the streamwise, wall-normal, and spanwise directions, respectively. L_x and L_z are the streamwise and spanwise domain lengths, respectively, nondimensionalized with the channel half width. Δx_f^+ and Δz_f^+ are the filter widths in the streamwise and spanwise directions in wall units based on the filter width criteria of Vasilyev *et al.* (Ref. 12) and Δy_f^+ is the filtered resolution in the wall-normal direction listed at both the channel wall and centerline. A range of Δy^+ resolutions near the centerline is given depending on the criteria used (Ref. 30).

Re_τ	N_x	N_y	N_z	Δx_f^+	Δz_f^+	Δy_f^+ (min)	Δy_f^+ (center)	L_x	L_z
180	64	64	64	71	24	0.24	20–25	4π	$\frac{4}{3}\pi$
180	96	96	96	71	24	0.16	20–25	4π	$\frac{4}{3}\pi$
180	128	128	128	71	24	0.12	20–25	4π	$\frac{4}{3}\pi$
395	64	64	64	78	39	0.53	50–60	2π	π
395	96	96	96	78	39	0.34	50–60	2π	π
395	128	128	128	78	39	0.25	50–60	2π	π
640	64	64	64	189	47	0.85	68–75	4π	π
640	96	96	96	189	47	0.55	68–75	4π	π
640	128	128	128	189	47	0.41	68–75	4π	π
640 (2)	128	64	128	94	24	0.32	80–90	4π	π
640 (2)	192	96	192	94	24	0.21	80–90	4π	π
640 (2)	256	128	256	94	24	0.16	80–90	4π	π

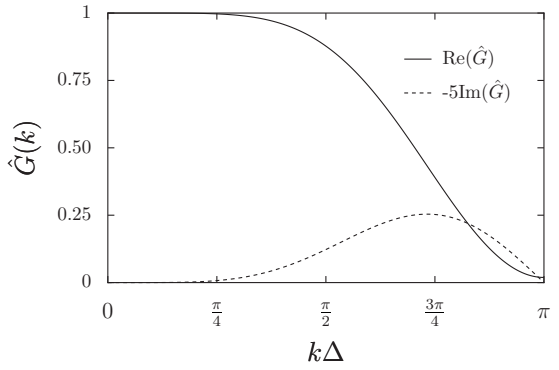

FIG. 3. Real and imaginary parts of Fourier transform of asymmetric filtering operator on a six-point stencil, $K=2$, $L=3$ as defined in Eq. (8).

wavenumbers, thereby reducing the influence of numerical errors on the simulation. It has been observed that the performance of the subfilter model is dependent on the filter type, particularly whether the filter is sharp or smooth.[20,21] It is expected that once the numerical error is sufficiently reduced, a grid-independent solution would be obtained.

Using this explicit filtering framework, it is possible to obtain solutions to the LES equations that are independent of the computational grid resolution. In practice, an explicit filter is applied to the LES equations to preserve only those scales larger than the filter width. The mesh can then be refined while keeping the filter width constant in order to make the contribution from numerical errors small enough in comparison with the resolved physical scales until a solution independent of the grid is achieved. This convergent solution is the "true" LES solution for the corresponding filter and the choice for the subfilter closure model.

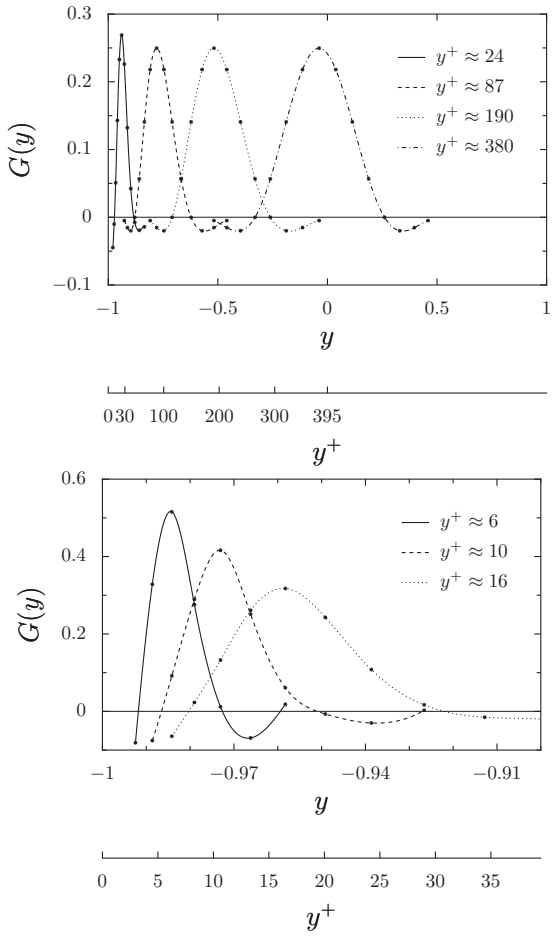

FIG. 4. Filtering operator in the wall-normal direction as a function of distance from the wall in physical and wall units in the outer layer (top) and inner layer (bottom) for a sample mesh at $\mathrm{Re}_\tau=395$.

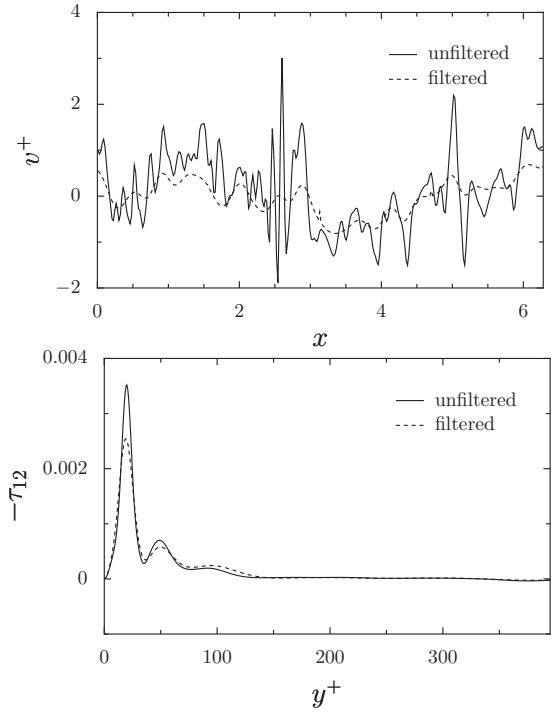

FIG. 5. Comparison of filtered and unfiltered instantaneous DNS profiles at $\mathrm{Re}_\tau=395$ of wall-normal velocity at $y^+\approx 30$ and fixed spanwise location (top) and $-\tau_{12}$ at a fixed stream- and spanwise locations (bottom).

The form of the LES equations in Eq. (5) is not new; Biringen and Reynolds[22] and Moin and Kim[23] both utilized this convective form in order to exploit the fact that the Leonard stresses could be directly calculated from the filtered velocity variable. However, explicit filtering was not applied in all three directions. Furthermore, this definition of explicitly filtered LES is different from the approach whereby primitive variables are explicitly filtered at the end of each time step. The latter is inconsistent with the governing equations for LES (for a more complete discussion, see Ref. 5). One potential drawback in using Eq. (5) is that it is not necessarily invariant under the Galilean transformation,[24] although it is possible to choose a subfilter stress model such that the invariance is restored.[17,10]

B. Numerical method

The test case considered in this study is the turbulent, planar channel flow.[23,25,26] This particular flow configuration is chosen because it is wall bounded, but the geometry is simple enough that the filter shape is uniform along the two homogeneous directions. The fourth-order finite difference scheme of Morinishi *et al.*[27] was implemented in a staggered mesh formulation, and the convective term is computed in its

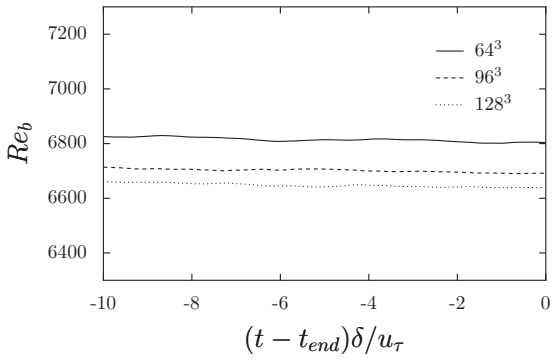

FIG. 6. Temporal evolution of $\mathrm{Re}_b=\bar{U}\delta/\nu$ at all grid resolutions at $\mathrm{Re}_\tau=395$ during the last $10(\delta/u_\tau)$ of statistical sampling, where $t_{\mathrm{end}}\delta/u_\tau\approx 30$ is the stopping time.

skew-symmetric form in order to discretely conserve kinetic energy. The time integration is performed using the fractional step method of Kim and Moin[28] (also Ref. 29) with the wall-normal diffusion terms treated implicitly with a Crank–Nicholson scheme, while the remaining terms were advanced with a second-order Adams–Bashforth scheme.

Fourth-order commuting, discrete filters derived by Vasilyev *et al.*[12] were used to perform the explicit filtering of the convective term. The discrete 1D filter used for the coarsest mesh was identical to the one implemented by Gullbrand,[10]

$$\bar{\phi}_i=-\tfrac{1}{32}\phi_{i-3}+\tfrac{9}{32}\phi_{i-1}+\tfrac{1}{2}\phi_i+\tfrac{9}{32}\phi_{i+1}-\tfrac{1}{32}\phi_{i+3}. \tag{10}$$

The filter coefficients for the medium and finer meshes are given in the Appendix. The three-dimensional filtering operation is then treated as a tensor product of the three 1D filters shown in Eq. (10). The grid distribution in the streamwise and spanwise directions is uniform with grid spacing Δ_p, but the wall-normal grid distribution is nonuniform. Because the filtering operation is derived to be applied in a uniformly distributed computational space, ζ, the nonuniform distribution of points in physical space results in a nonuniform filter width in the wall-normal direction. The distribution of grid points in the wall-normal direction is given by a hyperbolic tangent stretching function,

$$y_j=-\frac{\tanh[\gamma(1-2\zeta_j)]}{\tanh(\gamma)},\quad \zeta_j=\frac{j}{N_2},\quad \text{for } j=1,\ldots,N_2, \tag{11}$$

where N_2 and γ are the number of grid points in the wall-normal direction and a mesh stretching parameter, respectively. Figure 2 depicts the Fourier transform of the filter functions used for the channel simulations. As the mesh is refined from the coarsest mesh to finer meshes, the filter width in Eq. (10) remains fixed. The width of the filter with respect to the local grid spacing has been widely discussed.[30] Typically, the second-order moment of the filter is used as a measure of the width of a filter.[31] However, for filters that commute with orders of accuracy greater than two, the second-order moment is zero. Instead, all the filters are derived so that the transfer functions in the Fourier space are identical, thereby resolving the same scales on different grids (see Fig. 2). It can be seen that the filter shape in the Fourier space damps the amplitudes of the smaller scales and, therefore, behaves as a proper low-pass filter. Estimates of the local filter width have been suggested using either the $\hat{\Delta}$ such that $\hat{G}(\pi/\hat{\Delta})=1/2$ (Ref. 12) or based on the second moment

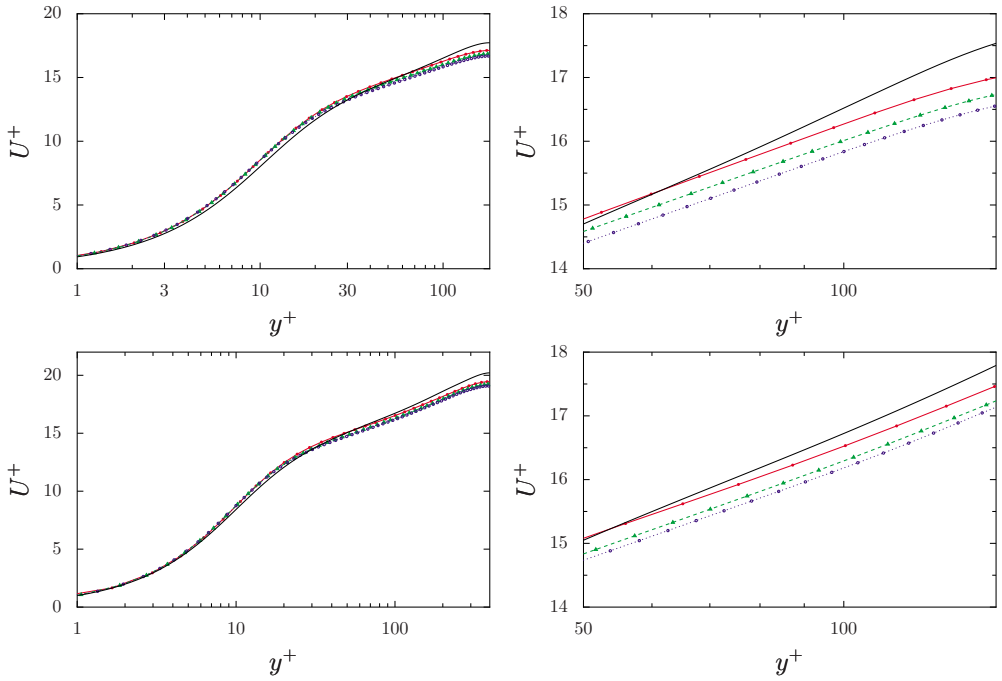

FIG. 7. (Color online) Mean streamwise velocity for a turbulent channel flow at $\mathrm{Re}_\tau=180$ (top row) and $\mathrm{Re}_\tau=395$ (bottom row) on 64^3 (–●–, red), 96^3 (---▲---, green), and 128^3 (···○···, blue) grids. The mean velocity profiles in the log layer are magnified for $\mathrm{Re}_\tau=180$ (top right) and $\mathrm{Re}_\tau=395$ (bottom right). The solid line denotes the filtered DNS solution and the insets show the convergence trends in the log layer.

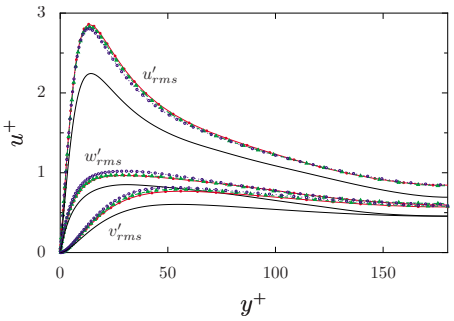

FIG. 8. (Color online) rms velocity profiles for a turbulent channel flow at $\mathrm{Re}_\tau=180$ using 64^3 (–●–, red), 96^3 (---▲---, green), and 128^3 (···○···, blue) grids. Solid lines denote filtered DNS solutions.

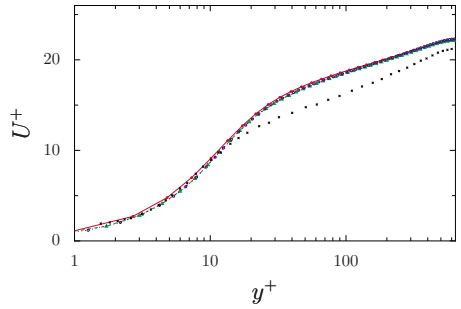

FIG. 10. (Color online) Mean streamwise velocity for a turbulent channel flow at $\mathrm{Re}_\tau=640$ on 64^3 (–●–, red), 96^3 (---▲---, green), and 128^3 (···○···, blue) grids. The symbols denote the experiment of Hussain and Reynolds (1970).

of the filter transfer function.[30] In this study, we have used the former criteria of Vasilyev *et al.*[12] for the homogeneous directions and have shown the results of both criteria for the wall-normal direction (see Table I). The nominal cutoff of the filters employed is chosen such that only the wavenumbers that can be accurately differentiated by the fourth-order finite difference scheme are preserved, even on the coarsest grid.

Asymmetric filtering is implemented in the wall-normal direction near the boundaries. The constraint that the filters commute to the same order as the truncation error is enforced near the boundaries, but the shape of the transfer function may be different at different grid resolutions. Because the filter stencil is no longer symmetric, the filtering operation introduces dispersion errors. Stolz *et al.*[17] attempted to minimize this dispersion error in their simulations by minimizing the imaginary part of the filter transfer function. In the inhomogeneous directions, the use of asymmetric filters is a necessity. An example of the asymmetric filter transfer function is shown in Fig. 3. Figure 4 shows the wall-normal filtering operator in physical space at three y locations for a sample mesh used for a $\mathrm{Re}_\tau=395$ channel flow simulation. The filtering operator is defined only at the points shown, and the line connecting the various points is shown only for visualization. The filtering kernel in physical space has regions where its value is negative, which is necessary for the filter to commute with differentiation to fourth order. These negative regions of the filter kernel in physical space are also observed in the standard sharp Fourier cutoff filter. The filter width varies as a function of wall-normal location and vanishes as the wall is approached. Although the effect of the filter is not immediately apparent in the turbulent statistics presented below, Fig. 5 shows the difference between the filtered and unfiltered wall-normal velocity and $-\tau_{12}$ for an instantaneous DNS flow field at $\mathrm{Re}_\tau=395$, where ν_t is the eddy viscosity and S is the strain rate tensor.

A dynamic Smagorinsky subfilter stress model is used in all channel flow simulations.[32] Because the subfilter stress term $\tau_{ij}=\overline{u_iu_j}-\overline{u}_i\overline{u}_j$ is different from the standard subgrid term in implicitly filtered LES, the Germano identity is modified as

$$L_{ij}=T_{ij}-\widetilde{\tau}_{ij}=\widetilde{\overline{u}_i\overline{u}_j}-\widetilde{\overline{u}}_i\widetilde{\overline{u}}_j, \tag{12}$$

where $\tilde{u}$ denotes a test-filtered quantity. The width of the test filter, Δ_T, for the dynamic Smagorinsky model is fixed at twice the width of the explicit filter, Δ_f, for all simulations. In order to be consistent with the spectral content of the other terms in the explicitly filtered LES equation, the subfilter stress contribution should also be filtered. Therefore, the modified Smagorinsky model[33,10] in Eq. (13) is used. The model parameter $C\Delta^2$ is computed dynamically using the least-squares method of Lilly,[34]

$$\tau_{ij}-\tfrac{1}{3}\tau_{kk}\delta_{ij}=-\overline{2(C\Delta^2)|\overline{S}|\overline{S}_{ij}}, \tag{13}$$

where $\overline{S}_{ij}=(1/2)[(\partial\overline{u}_i/\partial x_j)+(\partial\overline{u}_j/\partial x_i)]$ is the resolved strain rate tensor and $|\overline{S}|=(2\overline{S}_{kl}\overline{S}_{kl})^{1/2}$ is the magnitude of the resolved strain rate tensor.

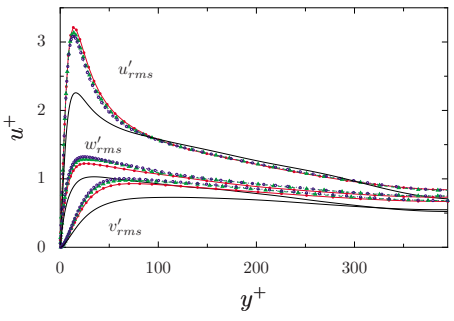

FIG. 9. (Color online) rms velocity profiles for a turbulent channel flow at $\mathrm{Re}_\tau=395$ using 64^3 (–●–, red), 96^3 (---▲---, green), and 128^3 (···○···, blue) grids. Solid lines denote filtered DNS solutions.

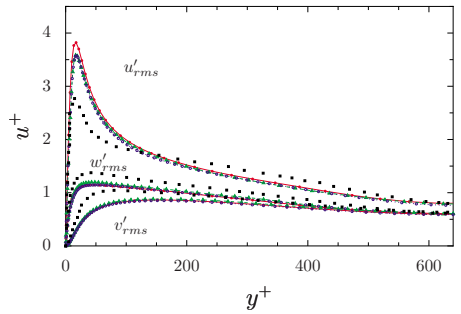

FIG. 11. (Color online) rms velocity profiles for a turbulent channel flow at $\mathrm{Re}_\tau=640$ using 64^3 (–●–, red), 96^3 (---▲---, green), and 128^3 (···○···, blue) grids, and unfiltered DNS (Abe *et al.*, 2001) (■).

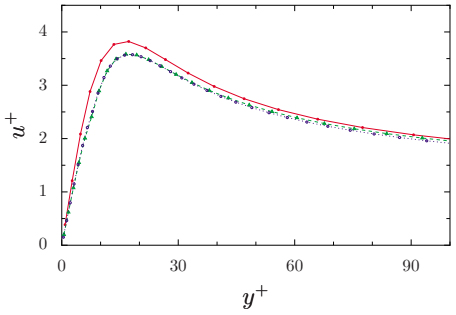

FIG. 12. (Color online) Streamwise rms velocity profiles for a turbulent channel flow at $\mathrm{Re}_\tau=640$ in the inner layer using 64^3 (–●–, red), 96^3 (---▲---, green), and 128^3 (···○···, blue) grids.

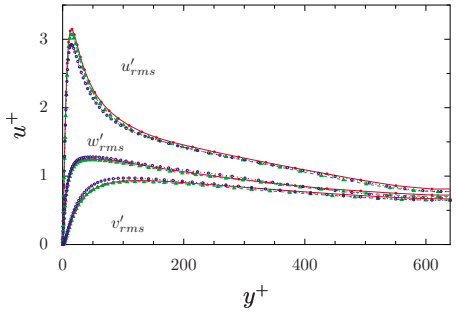

FIG. 14. (Color online) rms velocity profiles for a turbulent channel flow at $\mathrm{Re}_\tau=640$ using $128\times64\times128$ (–●–, red), $192\times96\times192$ (---▲---, green), and $256\times128\times256$ (···○···, blue) grids.

III. RESULTS AND DISCUSSION

Channel flow simulations are performed at $\mathrm{Re}_\tau=180$, 395, and 640 where a fixed pressure gradient is used to drive the flow in the channel. The Reynolds number, Re_τ, is based on the wall friction velocity, u_τ, and the channel half height, δ. At each Reynolds number, three LESs are performed with a fixed filter width while the mesh resolution is allowed to vary (Table I). At each Re_τ, a simulation on the coarsest grid was started from a log law profile perturbed with random numbers with amplitudes approximately 5% of the streamwise velocity. This initial field was allowed to evolve for a time of $10(\delta/u_\tau)$ so that turbulent structures could form. After this initial transient period, the solution on the coarse grid was interpolated onto the finer grids, and all grid levels were perturbed again with random numbers whose amplitudes were 5% of the streamwise velocity; this state is referred to as $t=0$. The simulations on all grids were allowed to evolve for another $10(\delta/u_\tau)$, and statistics were collected for a time period of at least $15(\delta/u_\tau)$ thereafter. Figure 6 shows the temporal evolution of $\mathrm{Re}_b=\bar{U}\delta/\nu$ (where $\bar{U}$ is the streamwise- and spanwise-averaged bulk velocity) over the last $10(\delta/u_\tau)$ time units during the statistical sampling. At each grid resolution, the deviation is less than 0.35% over this period and it is deemed that the statistics are sufficiently converged. The distribution of grid points in the wall-normal direction is described by the hyperbolic tangent stretching function, Eq. (11); the stretching parameter γ is fixed at 2.40 for all simulations unless otherwise noted. The Δy_f^+ at the channel wall slightly differs between simulations at the same Reynolds numbers because the filter width is forced to vanish at the first grid point away from the wall. However, the slight mismatch in filter width is limited to the viscous sublayer and its effect on the turbulent statistics is not significant.

The streamwise mean and the root mean square (rms) of the three velocity components are averaged in time and over horizontal planes. Figure 7 shows the mean streamwise velocity profiles for $\mathrm{Re}_\tau=180$ and $\mathrm{Re}_\tau=395$. The mean velocity profiles collapse between the two finer grid simulations on the 96^3 and 128^3 meshes. The DNSs at both of these Reynolds numbers are filtered to the same resolution as the corresponding LES. Figure 10 shows the mean streamwise velocity profile at $\mathrm{Re}_\tau=640$, and the collapse of the finer simulations is similar to those at $\mathrm{Re}_\tau=180$ and 395. At $\mathrm{Re}_\tau=180$ and 395, the filtered DNS mean streamwise velocity profile was nearly identical to the DNS and experimental data, and so the experiment of Hussain and Reynolds[35] is provided for reference in Fig. 10. Since the LES calculations have reached grid independence, the discrepancy between filtered DNS and the converged LES is attributed to the subfilter closure model.

Figures 8 and 9 show the rms velocity profiles for the streamwise, wall-normal, and spanwise directions at $\mathrm{Re}_\tau=180$ and 395, respectively. Near the channel centerline, the rms velocity profiles for the two finer LES calculations collapse well at both Reynolds numbers, similar to the behavior shown for the mean velocity. The collapse, however,

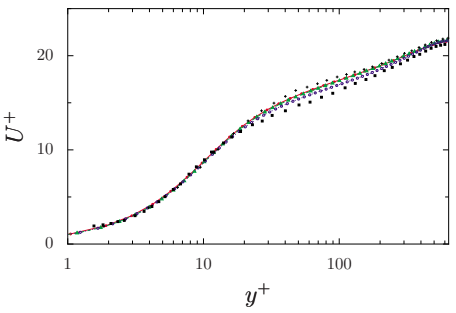

FIG. 13. (Color online) Mean streamwise velocity for a turbulent channel flow at $\mathrm{Re}_\tau=640$ on 64^3 (–●–, red), 96^3 (---▲---, green), and 128^3 (···○···, blue) grids. The symbols denote the experiment of Hussain and Reynolds (1970) (■) and the LES of Horiuti (1987) (+).

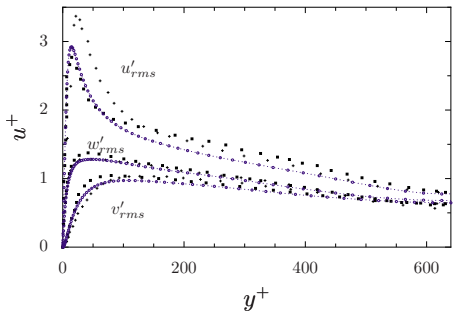

FIG. 15. (Color online) Comparison of rms velocity profiles at $\mathrm{Re}_\tau=640$ explicit filtered LES (···○···, blue), LES of Horiuti (1987) (+), and unfiltered DNS (Abe *et al.*, 2001) (■).

TABLE II. Integrated relative difference, Eq. (14), between intermediate (96^3 points) and fine (128^3) grid simulations for first- and second-order statistical quantities at $\mathrm{Re}_\tau=180$, 395, and 640. Re_b is the Reynolds number based on the averaged bulk velocity, and Re_{cl} is the Reynolds number based on the averaged centerline velocity.

Re_τ	$E(\bar{u})$ (%)	$E(\bar{u}'_{rms})$ (%)	$E(\bar{v}'_{rms})$ (%)	$E(\bar{w}'_{rms})$ (%)	$E(\mathrm{Re}_b)$ (%)	$E(\mathrm{Re}_{cl})$ (%)
180	0.9	0.8	2.6	2.1	0.9	1.0
395	0.7	0.7	1.3	0.9	0.8	0.8
640	1.0	0.9	2.3	1.2	0.6	0.7

is not as apparent in the near-wall peaks at both Reynolds numbers. Although the 1D filter transfer functions on varying grid resolutions are matched by minimizing their mean square difference, the filters do not match exactly over all wavenumbers. This problem is more pronounced near the wall where asymmetric filtering is employed; in the finest LES simulations using 128^3 grid points, the first seven grid points away from the wall require asymmetric filtering. Figure 11 shows all the rms velocity profiles for the channel flow at $\mathrm{Re}_\tau=640$. The profiles also converge for the two finer LES calculations, but there is an observable difference between the coarsest LES calculation and the grid-independent solution for u'_{rms} in the near-wall peak shown in Fig. 12.

The final three LES calculations listed in Table I at $\mathrm{Re}_\tau=640$ use a spatial filter different from that of the preceding calculations where wavenumbers that are contaminated with numerical error are filtered to a lesser extent. Figure 13 shows the mean streamwise velocity profiles for the three LES calculations compared against the LES of Horiuti[36] and the experiment of Hussain and Reynolds. The rms velocity profiles for all three grid resolutions are shown in Fig. 14. A collapse of the three rms profiles and the mean velocity profile within statistical scatter is observed away from the wall for $y^+>100$. However, convergence is not observed for the profiles in the region $y^+<100$. The overshoot in u'_{rms} in the near-wall region reduces as the mesh is refined at fixed filter width as the effect of numerical error is reduced. The scatter in the v'_{rms} and w'_{rms} profiles is less than 5% even in the near-wall region, but the near-wall regions have not converged to a grid-independent solution yet. The previous set of simulations at $\mathrm{Re}_\tau=640$ (Figs. 10–12) had shown convergent behavior even for $y^+<100$. Therefore, the lack of convergence for $y^+<100$ in Figs. 13 and 14 is because the filter used better preserves numerically contaminated scales than the filter used in the preceding calculations. It is expected that further grid refinement is necessary to obtain a fully converged solution. Figure 15 compares the rms velocity profiles from the most converged explicitly filtered LES ($256\times192\times256$) with rms predictions of Horiuti, and an unfiltered DNS.[37] For a fair comparison with the explicitly filtered LES, the DNS data should be filtered as was done at the lower Reynolds numbers, but the unfiltered DNS is provided as a reference. The explicitly filtered LES has similar predictions for the v'_{rms} and w'_{rms} quantities as Horiuti, but there is a pronounced difference in the grid-independent LES and Horiuti's calculations in the u'_{rms}, especially in the near-wall peak. The near-wall u'_{rms} overshoot on the less converged explicitly filtered LES solution ($128\times64\times128$) is close to the result from Horiuti.

Convergence of numerical methods is typically measured by computing the L_p error of a computed solution against an exact or reference solution. However, such a convergence trend is hard to infer from only three LES calculations. Instead, a measure of the integrated relative error is proposed to estimate the difference between the wall-normal profiles,

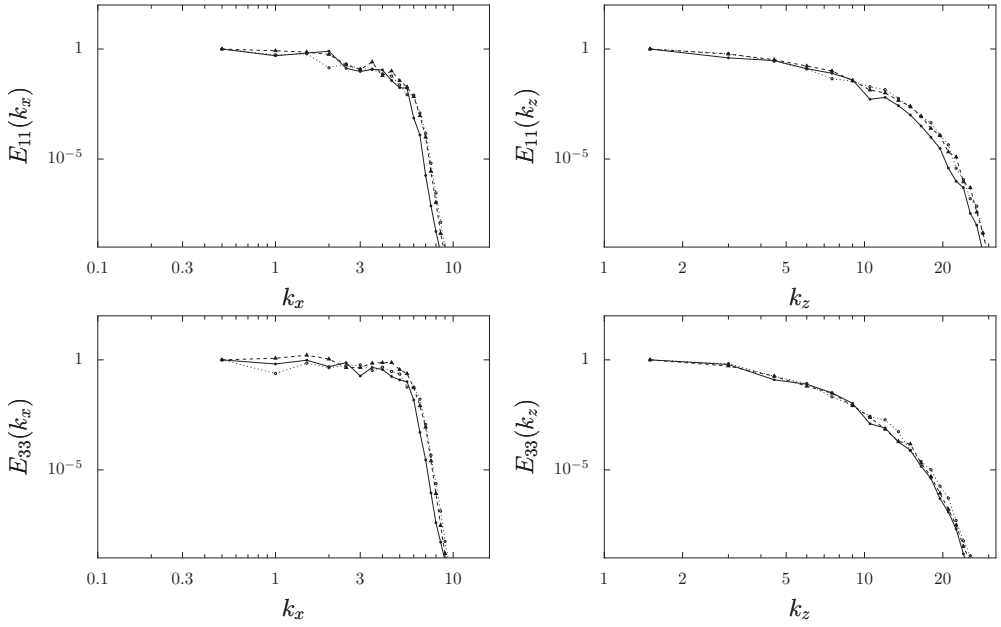

FIG. 16. One dimensional energy spectra, $E_{uu}(k_x)$ (top left), $E_{uu}(k_z)$ (top right), $E_{ww}(k_x)$ (bottom left), and $E_{ww}(k_z)$ (bottom right) for $\mathrm{Re}_\tau=180$ channel flow on 64^3 (–●–), 96^3 (---▲---), and 128^3 (···○···) grids at $y^+\approx180$.

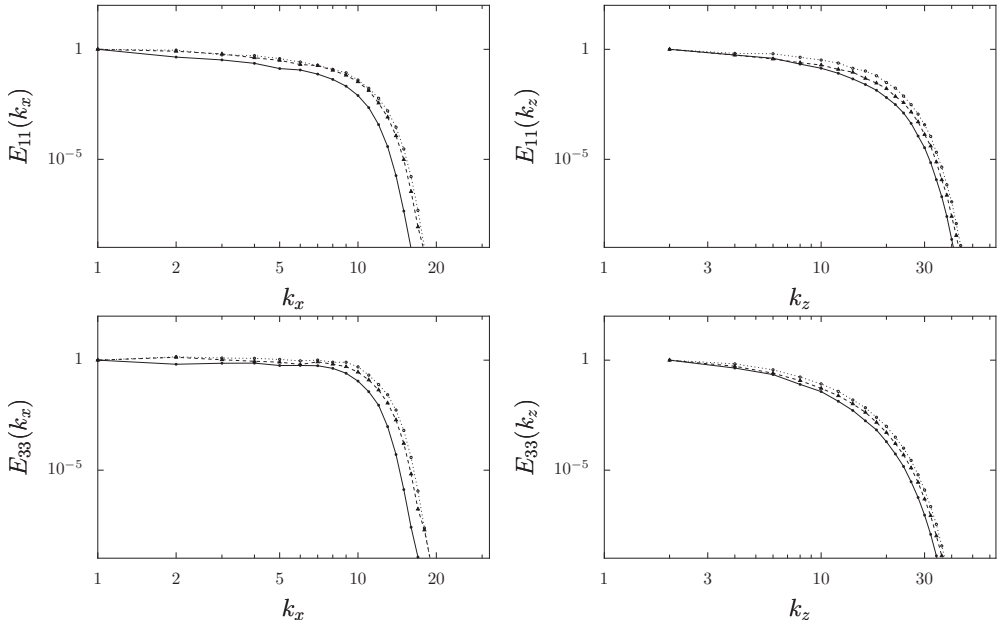

FIG. 17. One dimensional energy spectra, $E_{uu}(k_x)$ (top left), $E_{uu}(k_z)$ (top right), $E_{ww}(k_x)$ (bottom left), and $E_{ww}(k_z)$ (bottom right) for $\mathrm{Re}_\tau=395$ channel flow on 64^3 (–●–), 96^3 (---▲---), and 128^3 (···○···) grids at $y^+\approx 395$.

$$E(f_1,f_2)=\frac{1}{2}\int_{-1}^{1}\frac{|f_1(y)-f_2(y)|}{|f_2(y)|}dy. \tag{14}$$

Table II shows the relative differences in the wall-normal profiles between the simulations performed on the medium and fine meshes for all Reynolds numbers. The profiles for the first- and second-order statistics collapse to within a few percent, which is within the range of the statistical scatter, and therefore are grid independent.

One dimensional energy spectra in the streamwise and spanwise wavenumbers are also presented (Figs. 16–18). The nominal cutoff for all simulations using the filter width criteria suggested by Vasilyev *et al.*[12] are $k_x=8$ for $\mathrm{Re}_\tau=180$ and $k_x=16$ for $\mathrm{Re}_\tau=395$. Figures 16 and 17 are taken from the channel centerlines at $\mathrm{Re}_\tau=180$ and $\mathrm{Re}_\tau=395$, respectively; Fig. 18 shows the spectra near $y^+=30$ for the $\mathrm{Re}_\tau=395$ case. The 1D energy spectra collapse for the LES simulations on 96^3 and 128^3 grids, both at the centerline and closer to the wall. Because the falloff of the 1D energy spectra coincides with the nominal cutoff of the filters, the collapse of the first- and second-order statistics is attributed to the use of explicit filtering.

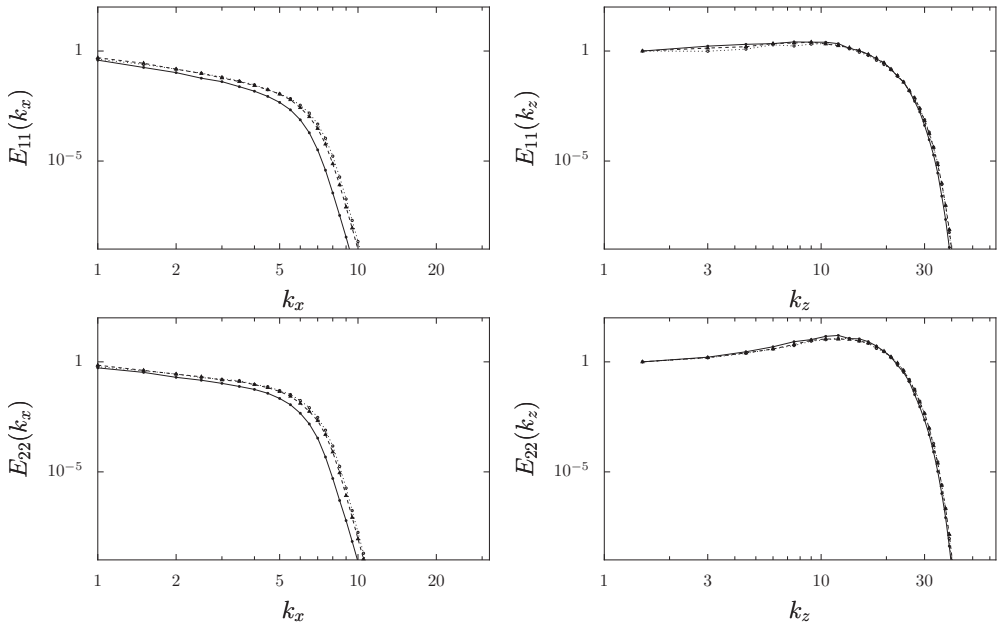

FIG. 18. One dimensional energy spectra, $E_{uu}(k_x)$ (top left), $E_{uu}(k_z)$ (top right), $E_{vv}(k_x)$ (bottom left), and $E_{vv}(k_z)$ (bottom right) for $\mathrm{Re}_\tau=395$ channel flow on 64^3 (–●–), 96^3 (---▲---), and 128^3 (···○···) grids at $y^+\approx 30$.

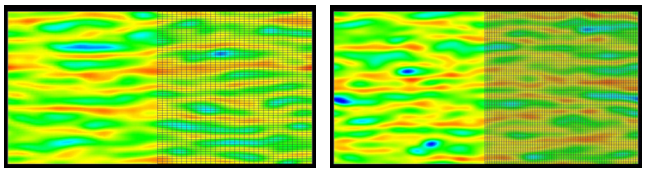

FIG. 19. (Color online) Wall shear stress, $\partial u/\partial y$, contours of an explicit filtered LES at $\mathrm{Re}_\tau=395$ for 64^3 (left) and 128^3 (right) grids in the x-z plane with the mesh overlaid. Qualitatively, the structure sizes are same between the two simulations, even though the mesh size of the 128^3 (right) LES is half the size of the 64^3 (left) LES in each direction.

Wall shear stress, $\partial\bar{u}/\partial y$, contours are presented in Fig. 19 for the coarsest and finest explicitly filtered LES calculations at $\mathrm{Re}_\tau=395$. The same contours for an implicitly filtered LES calculation using the same grid at the finest LES with 128^3 grid points are shown in Fig. 20. Some qualitative agreement in the size of the wall shear stress structures can be seen between the 64^3 and 128^3 explicitly filtered LES. The structures in the implicitly filtered LES equation show the presence of smaller scales and even small corrugations of the long streamwise streaks; these small-scale corrugations are not present in the explicitly filtered LES. The ensemble average of the $\tau_{12}=-2\nu_t\bar{S}_{12}$ contribution of the Smagorinsky model is computed at $\mathrm{Re}_\tau=395$ in Fig. 21. The convergence of the subfilter stresses is similar to the trends observed earlier for the first- and second-order statistics.

A few remarks are included regarding the additional computational cost of the explicitly filtered LES relative to the traditional implicitly filtered LES. It is difficult to assess the exact computational cost of the explicitly filtered LES as it is largely dependent on the characteristics of the filter employed, the choice of the subgrid/subfilter model, and the corresponding numerical implementation. For the present implementation, most of the increased computational cost arises from the dynamic computation of ν_t in the Smagorinsky model since the test filter required for the explicitly filtered LES requires a stencil wider than that of the test filter for an implicitly filtered LES along each coordinate direction. However, the time required to compute ν_t in both implicitly filtered and explicitly filtered LES is still small compared to the time required to solve the pressure Poisson equation or for implicit time advancement.

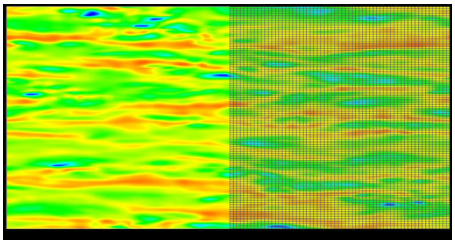

FIG. 20. (Color online) Wall shear stress, $\partial u/\partial y$, contours of an implicit filtered LES at $\mathrm{Re}_\tau=395$ for 128^3 grids in the x-z plane with the mesh overlaid.

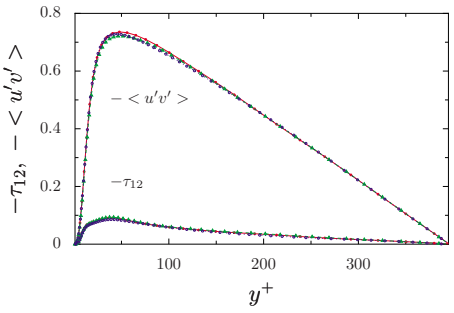

FIG. 21. (Color online) Ensemble averaged subfilter stress, $\tau_{12}=-2\nu_t\bar{S}_{12}$, and resolved Reynolds stress, $\langle u'v'\rangle$, at $\mathrm{Re}_\tau=395$ using 64^3 (–●–, red), 96^3 (---▲---, green), and 128^3 (···○···, blue) grids.

IV. CONCLUDING REMARKS

Grid-independent statistics and spectra for turbulent channel flow at different Reynolds numbers have been demonstrated in this study. The application of an explicit filter to the LES equations has enabled an unambiguous separation of the scales that are resolved in the simulation and those that must be modeled. Explicit filtering also offers hope of controlling the influence of numerical error in simulations, even if the magnitude of the truncation error is larger than the contribution of the smallest, dynamically relevant, physical scale η.

Moreover, the failure of the grid-independent LES solutions to converge to a filtered DNS can now be attributed directly to errors in the subfilter stress closure model. In the implicitly filtered LES framework, it was difficult to assess the fidelity of the closure model owing to the observed sensitivity of the subgrid model to numerical errors. The grid-independent solutions of the explicitly filtered LES equations suggest that they can be used to determine the performance of a particular subfilter stress model when compared with a filtered DNS or with experimental data.

ACKNOWLEDGMENTS

This work was supported by the Stanford Graduate Fellowship, the Department of Energy Computational Science Graduate Fellowship under Grant No. DE-FG02-97ER25308, and the Department of Energy PSAAP Program. Computational resources were provided by NASA-Ames Research Center and are gratefully acknowledged.

APPENDIX: ADDITIONAL FILTER COEFFICIENTS

The homogeneous filter coefficients for the explicit filter on the medium and fine meshes are listed below. The discrete form of the filter is given in Eq. (9), and only the weights, w_j, are shown below. The weights for the medium mesh are

$$w_0=\frac{457}{1367},\quad w_{\pm1}=\frac{1031}{3952},\quad w_{\pm2}=\frac{484}{4435},$$
$$w_{\pm3}=-\frac{30}{186\,421},\quad w_{\pm4}=-\frac{795}{31\,219},\quad w_{\pm5}=-\frac{123}{10\,658}, \tag{A1}$$

and for the finest mesh are

$$w_0 = \frac{260}{1043}, \quad w_{\pm 1} = \frac{17}{78}, \quad w_{\pm 2} = \frac{1579}{11\,201},$$
$$w_{\pm 3} = \frac{203}{3561}, \quad w_{\pm 4} = -\frac{10}{85\,099}, \quad w_{\pm 5} = -\frac{168}{8287}, \tag{A2}$$
$$w_{\pm 6} = -\frac{745}{47\,852}, \quad w_{\pm 7} = -\frac{117}{25\,400}.$$

[1] K. Mahesh, G. Constantinescu, S. Apte, F. Ham, and P. Moin, "Large-eddy simulation of reacting turbulent flows in complex geometries," ASME J. Appl. Mech. **73**, 374 (2006).
[2] D. You, M. Wang, P. Moin, and R. Mittal, "Large eddy simulation analysis of mechanisms for viscous losses in turbomachinery tip-clearance flow," J. Fluid Mech. **586**, 177 (2007).
[3] D. You, F. Ham, and P. Moin, "Discrete conservation principles in large-eddy simulation with application to separation control over an airfoil," Phys. Fluids **20**, 101515 (2008).
[4] R. S. Rogallo and P. Moin, "Numerical simulation of turbulent flow," Annu. Rev. Fluid Mech. **16**, 99 (1984).
[5] T. S. Lund, "The use of explicit filters in large eddy simulation," Compos. Math. **46**, 603 (2003).
[6] A. G. Kravchenko and P. Moin, "Numerical studies of flow over a circular cylinder at Re_d=3900," Phys. Fluids **12**, 403 (2000).
[7] J. Meyers and P. Sagaut, "Is plane-channel flow a friendly case for the testing of large-eddy simulation subgrid-scale models?" Phys. Fluids **19**, 048105 (2007).
[8] A. G. Kravchenko and P. Moin, "On the effect of numerical errors in large eddy simulation," J. Comput. Phys. **131**, 310 (1997).
[9] F. K. Chow and P. Moin, "A further study of numerical errors in large eddy simulation," J. Comput. Phys. **184**, 366 (2003).
[10] J. Gullbrand, "Grid-independent large-eddy simulation in turbulent channel flow using three-dimensional explicit filtering," *Center for Turbulence Research Annual Research Briefs* (Center for Turbulence Research, Stanford, CA, 2003), pp. 331–342.
[11] B. J. Geurts and D. D. Holm, "Regularization modeling for large-eddy simulation," Phys. Fluids **15**, L13 (2003).
[12] O. V. Vasilyev, T. S. Lund, and P. Moin, "A general class of commutative filters for LES in complex geometries," J. Comput. Phys. **146**, 82 (1998).
[13] A. L. Marsden, O. V. Vasilyev, and P. Moin, "Construction of commutative filters for LES on unstructured meshes," J. Comput. Phys. **175**, 584 (2002).
[14] A. Haselbacher and O. V. Vasilyev, "Commutative discrete filtering on unstructured grids based on least-squares techniques," J. Comput. Phys. **187**, 197 (2003).
[15] S. B. Pope, "Ten questions concerning the large-eddy simulation of turbulent flows," New J. Phys. **6**, 35 (2004).
[16] G. S. Winckelmans, A. A. Wray, O. V. Vasilyev, and H. Jeanmart, "Explicit-filtering large-eddy simulation using the tensor-diffusivity model supplemented by a dynamic Smagorinsky term," Phys. Fluids **13**, 1385 (2001).
[17] S. Stolz, N. A. Adams, and L. Kleiser, "An approximate deconvolution model for large-eddy simulation with application to incompressible wall-bounded flows," Phys. Fluids **13**, 997 (2001).
[18] N. M. Mansour, P. Moin, W. C. Reynolds, and J. H. Ferziger, "Improved methods for large-eddy simulation of turbulence," *Turbulent Shear Flows I* (Springer, Berlin, 1979), pp. 386–401.
[19] P. Moin, *Fundamentals of Engineering Numerical Analysis* (Cambridge University Press, Cambridge, 2001).
[20] G. De Stefano and O. V. Vasilyev, "Sharp cutoff versus smooth filtering in large eddy simulation," Phys. Fluids **14**, 362 (2002).
[21] U. Piomelli, P. Moin, and J. H. Ferziger, "Model consistency in large eddy simulation of turbulent channel flows," Phys. Fluids **31**, 1884 (1988).
[22] S. Biringen and W. C. Reynolds, "Large-eddy simulation of the shear-free turbulent boundary layer," J. Fluid Mech. **103**, 53 (1981).
[23] P. Moin and J. Kim, "Numerical investigation of turbulent channel flow," J. Fluid Mech. **118**, 341 (1982).
[24] C. G. Speziale, "Galilean invariance of subgrid-scale stress models in the large-eddy simulation of turbulence," J. Fluid Mech. **156**, 55 (1985).
[25] J. Kim, P. Moin, and R. D. Moser, "Turbulent statistics in a fully developed channel flow," J. Fluid Mech. **177**, 133 (1987).
[26] R. D. Moser, J. Kim, and N. M. Mansour, "Direct numerical simulation of turbulent channel flow," Phys. Fluids **11**, 943 (1999).
[27] Y. Morinishi, T. S. Lund, O. V. Vasilyev, and P. Moin, "Fully conservative higher order finite difference schemes for incompressible flow," J. Comput. Phys. **143**, 90 (1998).
[28] J. Kim and P. Moin, "Application of a fractional-step method to incompressible Navier–Stokes equations," J. Comput. Phys. **59**, 308 (1985).
[29] J. K. Dukowicz and A. S. Dvinsky, "Approximate factorization as a high order splitting for incompressible flows," J. Comput. Phys. **102**, 336 (1992).
[30] T. S. Lund, "On the use of discrete filters for large eddy simulation," *Center for Turbulence Research Annual Research Briefs* (Center for Turbulence Research, Stanford, CA, 1997, pp. 83–95.
[31] A. Leonard, "On the energy cascade in large-eddy simulations of turbulent flows," Thermosciences Division, Stanford University Technical Report No. TF-1, 1973.
[32] M. Germano, U. Piomelli, P. Moin, and W. H. Cabot, "A dynamic subgrid-scale eddy viscosity model," Phys. Fluids A **3**, 1760 (1991).
[33] D. Carati, G. Winckelmans, and H. Jeanmart, "On the modelling of the subgrid-scale and filtered-scale stress tensors in large-eddy simulation," J. Fluid Mech. **441**, 119 (2001).
[34] D. K. Lilly, "A proposed modification of the Germano subgrid-scale closure method," Phys. Fluids A **4**, 633 (1992).
[35] A. K. M. F. Hussain and W. C. Reynolds, "The mechanics of a perturbation wave in turbulent shear flow," Thermosciences Division, Stanford University Technical Report No. FM-6, 1970.
[36] K. Horiuti, "Comparison of conservative and rotational forms in large eddy simulation of turbulent channel flow," J. Comput. Phys. **71**, 343 (1987).
[37] H. Abe, H. Kawamura, and Y. Matsuo, "Direct numerical simulation of a fully developed turbulent channel flow with respect to the Reynolds number dependence," ASME J. Fluids Eng. **123**, 382 (2001).